Unsupervised respiratory signal extraction from ungated cardiac magnetic resonance imaging at rest and during exercise

Felipe Novillo[1], Simon Van Eyndhoven[2,3], Jonathan Moeyersons[2,3], Jan Bogaert[4], Guido Claessen[5], André La Gerche[6], Sabine Van Huffel[2,3] and Piet Claus[1]

[1] KU Leuven, Department of Cardiovascular Sciences, Cardiovascular Imaging and Dynamics, Leuven, Belgium
[2] KU Leuven, Department of Electrical Engineering (ESAT), STADIUS Center for Dynamical Systems, Signal Processing and Data Analytics, Leuven, Belgium
[3] imec, Leuven, Belgium
[4] KU Leuven, Department of Imaging and Pathology, Translational MRI unit, Leuven, Belgium
[5] KU Leuven, Department of Cardiovascular Sciences, Cardiology unit, Leuven, Belgium
[6] Baker Heart and Diabetes Institute, Melbourne, Vic, Australia

E-mail: piet.claus@kuleuven.be

Abstract. We propose and evaluate a method to estimate a respiratory signal from ungated cardiac magnetic resonance (CMR) images. Ungated CMR images were acquired in 5 subjects who performed exercise at different intensity levels under different physiological conditions while breathing freely. The respiratory motion was estimated by applying principal components analysis (PCA). A sign correction procedure was developed to correctly define inspiration and expiration, based on either tracking of the diaphragmatic motion or estimation of the lung volume or a combination of both. Evaluation was done using a plethysmograph signal as reference. There was a good correspondence between the plethysmograph and the estimated respiratory signals. Respiratory motion was effectively captured by one of the PCA components in 88% of the cases. Moreover, the proposed method successfully estimated the respiratory phase in 91% of the evaluated slices. The pipeline is robust, admitting a slight decline in performance with increased exercise intensity. Respiratory motion was accurately estimated by means of PCA and the application of a sign correction procedure. Our method showed promising results even for acquisitions during exercise where excessive body motion occurs. The proposed method provides a way to extract the respiratory signal from ungated CMR images, at rest as well as during exercise, in a fully unsupervised fashion, which may reduce the clinician's workload drastically.

Keywords: Respiratory Motion Extraction, Principle Component Analysis, Exercise Cardiac Magnetic Resonance Imaging.

1. Introduction

On the one hand, respiratory motion is often considered a nuisance in medical imaging, leading to artifacts and inaccurate quantification. Breath-holding or (retrospective) respiratory gating techniques are widely used to reduce the influence of respiratory motion. On the other hand, the interaction of the respiration with the cardiovascular system can also yield useful information on cardiac function [1] and studying the interaction of respiration and cardiac function during exercise is of particular interest. Real-time ungated cine imaging protocols have been developed over the years to capture cardiac and respiratory motion during free breathing yielding accurate and reproducible measurements of cardiac output and volumes at rest and during high intensity exercise [2]. However, manual identification of respiratory phases is time consuming and automated methods are highly desired. External devices, that measure the displacement of the chest or abdomen, are commonly used to capture respiratory motion. This signal is then used subsequently to reconstruct images or trigger image acquisition according to a specific respiratory phase. In some patients they do not always accurately represent the real respiratory motion [3]. However, respiratory motion is inherently present in the ungated real-time cine images and data driven techniques could allow extraction of the respiratory signal from the images alone, avoiding the plethysmography. Several algorithms which remove artifacts and diminish the blurring effect on the images have been the main subject of research for acquisitions where breath-holding technique is unfeasible [4] or subjects are unable to hold their breath for a prolonged period of time [5]. In our application however, extraction of the respiratory signal itself is of interest. For example, in [1], the determination of inspiration and expiration phases is essential to accurately interpret the interaction between respiration and right versus left ventricular volumes at rest and during exercise.

The extraction of the respiratory motion from the data itself, for subsequent motion correction, has been the principal aim of several studies and numerous strategies have been developed for different imaging modalities such as positron emission tomography (PET) [6, 7, 8], computed tomography (CT) [9] or magnetic resonance imaging (MRI) [5, 10, 11, 12, 13, 14, 15].

A particularly appealing approach used principal component analysis (PCA) to dynamic sinograms of in PET/CT imaging [16]. The estimated respiratory signal was derived from the first principal component (PC) and showed high correlation with the corresponding external device measurement. An advantage of this method is the reduced processing time compared to previous studies. However, PCA could be influenced by other types of motion which are not related to respiration. Thus, prior knowledge is needed to determine the principal component that corresponds to the respiratory motion. This has been addressed by Bertolli *et al.* [4], where the respiration-related principal component was automatically identified by spectral analysis.

In addition, due to the nature of the PCA the sign of the estimated signal is arbitrary. Hence, proper determination of the sign is needed to accurately identify

inspiration and expiration. Methods to overcome this were applied to PET raw data assuming that respiration generates a cranio-caudal motion of the internal organs [4].

In this work, starting from the images optimized for free-breathing ungated real-time cine imaging during intense exercise [2], we propose an unsupervised data-driven method to extract the respiratory signal from ungated cardiac MRI (CMR) at rest and during exercise based on PCA. In addition, we implement a sign correction procedure to determine the correct respiratory phase.

2. Methods

2.1. Subjects

Data from 5 healthy volunteers were used in the present study and selected based on having optimal and reliable plethysmograph data during all scans. All subjects performed an exercise protocol with four exercise intensity levels (section 2.2) breathing room air. At each level a CMR scan (section 2.3) was performed. The same exercise protocol was repeated under two different physiological conditions, i.e. low oxygen breathing (Hypoxia) and pulmonary vasodilation (Sildenafil). Acquisitions could not be performed at maximal intensity (66%) during hypoxia, due to the physiological constraint of low oxygen, not enabling this exercise level in normal subjects. An elaborate description can be found in [17].

For the purpose of our study, this yielded a large range of respiration modes obtained during exercise to validate our algorithm. The total of 55 scans (11 scans per volunteer) were used as follows. Five scans during rest and breathing room air were used to develop the algorithm. The algorithm was than tested on the remaining datasets, i.e. 10 scans at rest, 15 at 25%, 15 at 50% and 10 at 66% of maximal exercise capacity, yielding 50 scans (representing 898 SAX slices in 5 volunteers). The performance of the algorithm was further analysed per exercise intensity level.

2.2. Exercise protocol

The day before the CMR, the subject performed a maximal exercise test on an upright cycle ergometer (ER900 and Oxycon, Alpha, Jaeger, Germany). This test used a 50W resistance level as the initial intensity and increments of 25W/min were applied until exhaustion. These results were used to determine the workloads during the CMR on a supine cycle ergometer (Lode, Groningen, The Netherlands). The resistance was adjusted according to the data obtained from the cardiopulmonary test, thus exercise intensities were determined as rest, 25%, 50% and 66% of the maximal intensity.

2.3. MRI acquisition protocol

A scan consists of a short axis (SAX) stack of ungated CMR images acquired using 1.5T scanner (Achieva, Philips Medical Systems, Best, The Netherlands) with a 5-element phased-array coil. Steady-state free-precession cine imaging was performed

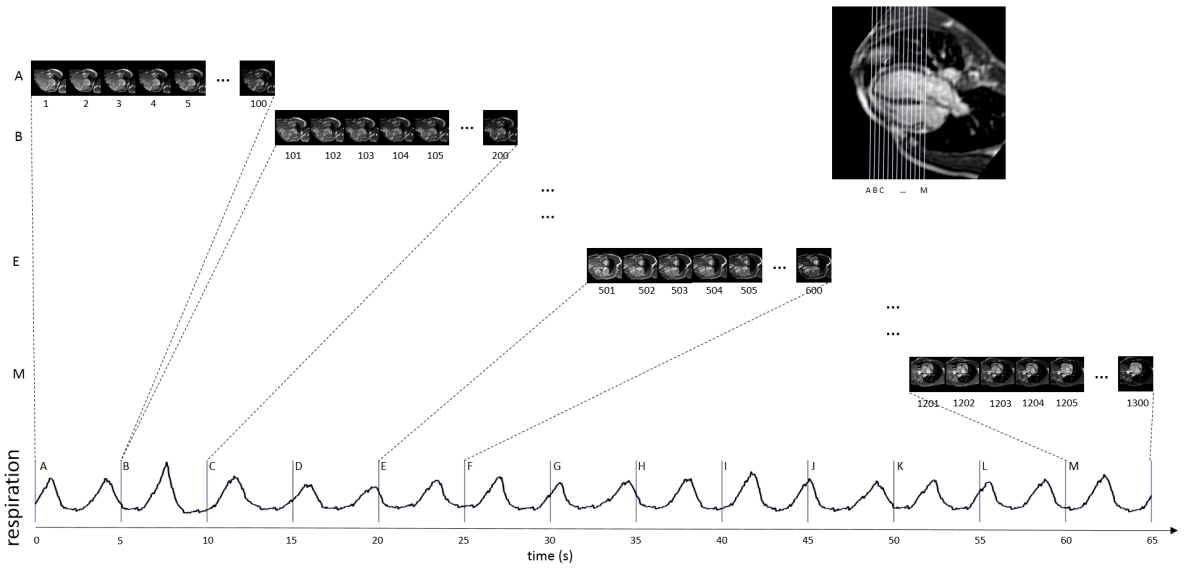

Figure 1. Ungated real-time SAX cine images are consecutively acquired for all slices covering both ventricles during free breathing with sufficient frames per slice to capture a full cardiac cycle.

without cardiac gating. SAX images were acquired consecutively from apex to base (Fig. 1) covering both ventricles. Imaging parameters were as follows: field of view, 320×260 mm (approximately); matrix size, 128×128 or 144×144; flip angle, echo time and repetition time were 50, 0.9 ms ans 1.8 ms; SENSE factor, 2 (Cartesian k-space undersampling). For each short slice sufficient images were acquired to capture at least one complete respiratory cycle. Typically 100 consecutive frames at rest and 60 at maximal intensity. (Fig. 1). During each scan, the respiratory signal was acquired by a plethysmograph and synchronized with each subject dataset using in-house-developed software (RightVol, KULeuven, Belgium). A detailed protocol has been described in [2].

2.4. Principle component representation

During acquisition, the cardiac MR images capture motion from the beating of the heart (∼1-2 Hz) and respiration (∼0.1-0.4 Hz). This latter motion component is what we aim to extract from the data. We can regard the set of cardiac MR images as a linear superposition of time-varying fluctuations due to the heartbeat, breathing, other body motion, scanner drift, and noise. It is intuitive to think about this in terms of a voxel in the lungs near e.g. the diaphragm: during a breathing cycle, the diaphragm (with a high intensity in the MR image) will move into the voxel and again out of it (at that time, the voxel will be filled with air, with a low MR intensity). This can be expressed through the following model:

$$X(v,t) = \bar{X}(t) + \sum_{k=1}^{K} p_k(v) w_k(t) + \varepsilon(v,t,K) \quad (1)$$
$$v = 1...V, t = 1...T$$

$$X = \bar{X} + PW + \varepsilon \quad (2)$$

In which the measured data X at every voxel v and time point t is a sum of contributions from $k = 1...K$ components p_k, weighted by relative intensities w_k and the mean of the data ($\bar{X}(t)$). Here K is the maximal number of PCA components considered to represent the data. Every row of the matrix W contains the weights (coefficients) for one principal component or source of temporal fluctuation, and the matrix P contains the principal components scores, which represents the data in X in the principal component space (i.e. the new basis vectors).

During the acquisition protocol (Fig. 1), different slices are scanned in separate, non-overlapping time periods of several seconds. Hence, data from different slices were processed separately, as both the set of variables (time points) and observations (voxels) were disjoint. To construct the data matrix X, all the frames from a particular slice were reshaped as column vectors and concatenated. Before applying the PCA algorithm, the matrix X was normalized to obtain zero mean and a standard deviation equal to one. Principal components weights computed for each of the slices were concatenated to obtain a signal corresponding to the entire stack of images of each acquisition. A Savitzky-Golay filter (5th order, window length= frames-1) was applied to the PCs to reduce noise and remove high frequency components. Fig. 2(a) shows an example of the weights corresponding to the first three principal components.

Given that respiration is a major source of variation in voxel intensity during a free breathing ungated acquisition, we expect that the effect of respiration can be captured in at least one of the first PC weights w_k.

To determine which of the first three PCA weights corresponds to respiration, a spectral analysis was performed. Fig. 2(b) shows the amplitude of the power spectra $S_k(f) = |\hat{w}_k(f)|$, (where $\hat{w}$ represents the fast Fourier transform (FFT) of the signal at frequency (f)) computed for the first three PCs, as described in [4]. The second component showed the most power within the respiratory frequency range [0.1, 0.4] Hz and its power spectrum corresponded well with the power spectrum of the plethysmograph signal (Fig. 2(c)). This yielded the rationale to work with the second PC to derive an image based respiratory signal. We will refer to the second PC signal as the respiration-related component (RRC).

2.5. Sign correction

The RRC provides an estimate of the respiratory signal. However, the sign of the signal indicating inspiration or expiration cannot be uniquely retrieved by PCA, as both

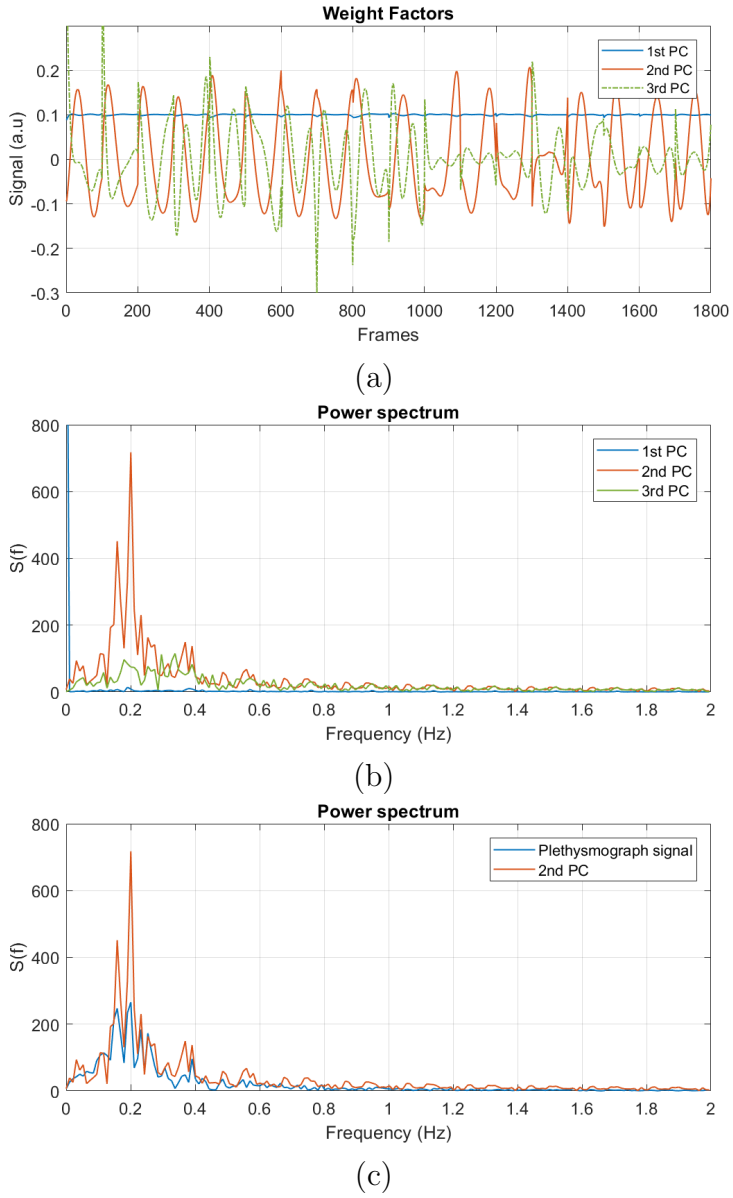

Figure 2. (a) Weights corresponding to the first three principal components. (b) Power spectrum of the PCs. (c) Power spectrum of the respiration-related component (RRC) and the plethysmograph signal.

inspiration and expiration yield similar variation in the data. Therefore, an additional sign determination is required in order to obtain a respiratory signal in which inspiration and expiration correspond to positive and negative peaks respectively. We implemented and compared two methods for sign correction.

2.5.1. Estimation of diaphragmatic motion. We adapted the 1D registration method of [4, 7] used for PET data. First a reference region of interest (ROI) was defined centered on the lung-diaphragm area. Hereto,the middle slice of the SAX stack was analyzed, since it always contains a large portion of the diaphragm. The frame corresponding to



(a) (b)

Figure 3. (a) Zero-crossing frame used to define the region of interest. (b) Same frame reconstructed using the RRC. The rectangle represents the ROI.

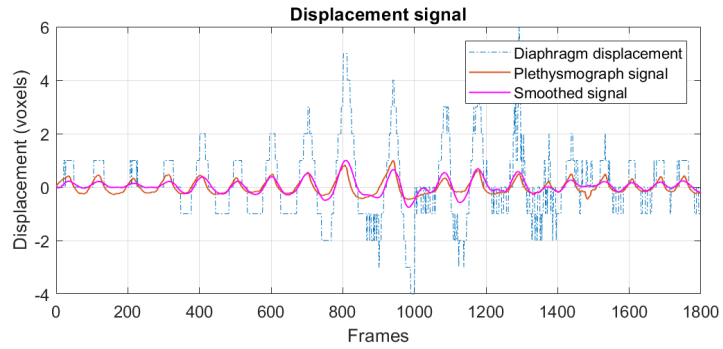

(a)

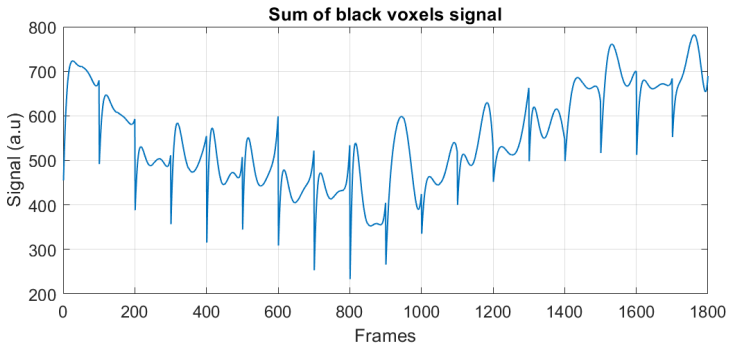

(b)

Figure 4. (a) Displacement signal. (b) Signal corresponding to the sum of the black voxels within the ROI.

the zero crossing of the RRC signal for that particular slice was considered (Fig. 3 (a)). The region of maximal respiratory motion was determined as the maximal absolute intensity voxel on the image reconstructed from the RRC only at the zero crossing (Fig. 3 (b)). The ROI was defined as a rectangle of 30 voxels wide and half of the image height (Fig. 3).

The same reference ROI was defined on all other slices at the frame determined by the zero crossing of the RRC in that slice. For each frame in the slice the motion was estimated by analyzing the 2D correlation coefficient between the reference ROI in the

reference frame and a sliding ROI. The displacement of the diaphragm occurs in the cranio-caudal direction, hence the sliding ROI was only displaced in this direction within a range of -12 to +12 voxels, corresponding to a maximum displacement of -31.2mm to +31.2mm. The direction of the diaphragm displacement for each frame corresponds to the highest correlation. The obtained value corresponds to the number of voxels of displacement regarding the reference position. Fig. 4(a) illustrates the obtained displacement signal and the plethysmograph signal. A smoothed displacement signal is also shown, where the similarity with the plethysmograph signal can be observed. A Savitzky-Golay filter (5th order, window length=frames-1) was applied to smooth the displacement signal.

2.5.2. Lung volume estimation As a second method to determine the sign of the RRC corresponding to respiration, the reference ROI defined above was kept fixed and the voxels in this ROI for all frames were thresholded using a voxel intensity of 40. Within this ROI black voxels are mostly related to lung, and a change of black voxel count correlates to a change lung volume. An increase in number of black voxels corresponds to inspiration. Before thresholding a median filter with a 5-by-5 neighborhood was applied to each frame to increase the signal to noise ratio of the image. The threshold was empirically determined by analyzing the histogram of the images and maximizing the segmentation of lung tissue. Fig. 4(b) shows the signal obtained from the segmentation procedure smoothing with a Savitzky-Golay filter (5th order, window length= frames-1).

Sign correction was performed slice-wise using the information of the RRC and both the diaphragm displacement and the sum of the black voxels signals. Pearson correlation coefficients were computed between the RRC signal and the other two signals obtained with the procedure explained before. A correlation threshold of 0.7 between the estimated and the displacement signals was defined, which corresponds to a high correlation between both signals. If the correlation coefficient is higher or equal to the defined threshold value the sign of the respiratory signal remains the same, whereas if correlation is lower or equal to -0.7 the estimated signal corresponding to that slice is reversed. When the absolute value of the correlation is lower than 0.7, then the correlation between the estimated signal and the sum of the black voxels signal is computed. In this case, the estimated signal will be reversed when the correlation coefficient is negative, otherwise the sign of the estimated respiratory signal remains the same. The final signal derived from the sign correction process was filtered using a Savitzky-Golay filter (5th order, window length= frames-1) to remove discontinuities between slices and to obtain a smooth signal to increase signal to noise ratio.

2.6. Reliability measures

To estimate the reliability of the algorithm, without using the ground truth plethysmograph signal, we defined reliability measures based on the correlation coefficients between the RRC and the displacement signal ρ_D and the RRC and "the

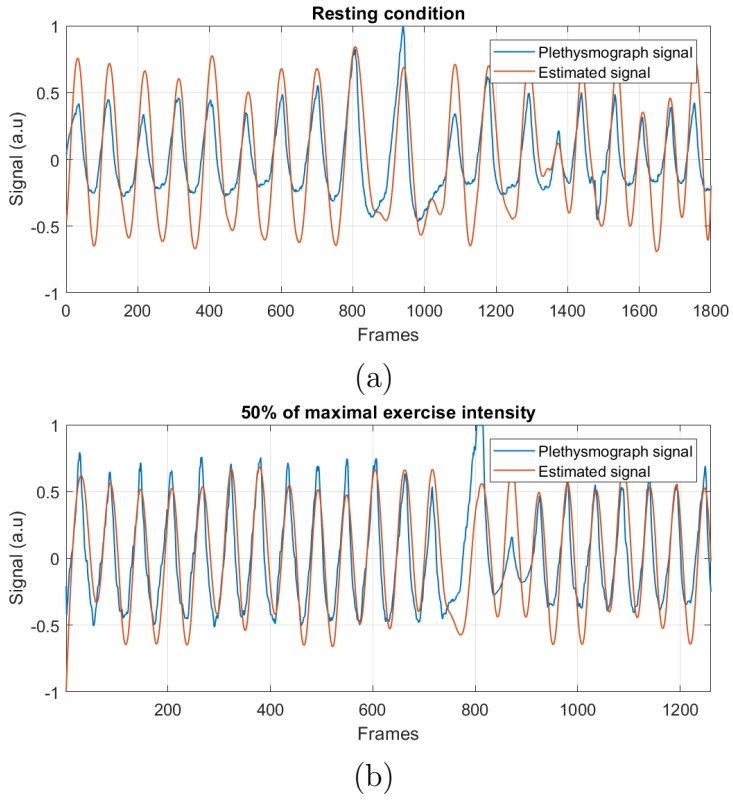

Figure 5. Estimated respiratory signal at (a) resting condition and (b) 50% of maximal exercise intensity. Both figures correspond to the same subject.

sum of black voxels" signal ρ_B. These correlation coefficients were calculated per slice. The following seven reliability measures were evaluated:

$$\begin{aligned}
\mathcal{R}^1 &= \rho_D\,, \\
\mathcal{R}^2 &= \rho_B\,, \\
\mathcal{R}^3 &= \text{mean}\{\rho_D, \rho_B\}\,, \\
\mathcal{R}^4 &= \max\{\rho_D, \rho_B\}\,, \\
\mathcal{R}^5 &= \min\{\rho_D, \rho_B\}\,, \\
\mathcal{R}^6_{t_D} &= \begin{cases} \rho_D & \text{if } \rho_D \geq t_D \\ \rho_B & \text{if } \rho_D t_D \end{cases}\,, \\
\mathcal{R}^7_{t_B} &= \begin{cases} \rho_B & \text{if } \rho_B \geq t_B \\ \rho_D & \text{if } \rho_B t_B \end{cases}
\end{aligned} \tag{3}$$

For each measure, receiver operating characteristics (ROC) analysis was performed to determine the optimal threshold, area under the curve (AUC) and sensitivity and specificity to detect erroneous respiratory signals. Optimal t_D and t_B were determined by maximizing the AUC for $\mathcal{R}^6$ and $\mathcal{R}^7$ resp. in repeated ROC analyses with incremental values of t_D and t_B resp.

Table 1. Percentage of success of the data-driven respiratory trace extraction at each exercise intensity and for each sign correction method applied. Number of scans and slices per exercise intensity are also included.

Exercise intensity	Scans	Slices	Combined	Displacement	Sum black voxels
Rest	10	180	96%	96%	89%
25%	15	270	92%	92%	87%
50%	15	270	88%	88%	86%
66%	10	178	87%	89%	87%
TOTAL	50	898	91%	89%	87%

2.7. Evaluation

The plethysmograph signal was defined as the ground truth against which to compare the results obtained from the algorithm.

To evaluate the performance of the proposed algorithm we considered several metrics.

Direct comparison of signal wave forms (metric a). For each completed scan, the final estimated respiratory signals were correlated to the plethysmograph signal. A correlation coefficient greater than 0.7 was considered a good result.

Sign correction performance (metric b). The percentage of slices were the sign was correctly estimated and the estimated signal was in phase with the plethysmograph data was assessed for each intensity level.

Respiratory frame estimation performance (metric c). As a last measure frames corresponding to the peaks of the respiratory signals and thus defining end-inspiration and end-expiration were compared to the plethysmograph derived peaks. The differences between the peaks in number of frames was quantified for each exercise level.

A further evaluation the different components of the pipeline (i.e. the PCA and the different sign correction procedures) were performed subsequently. To assess the performance of the PCA alone, the RRC was artificially sign corrected using the ground truth plethysmograph signal (optimal PCA) - representing the algorithm when the sign correction algorithm would be faultless - metrics (a) and (b) above were evaluated. In addition, metrics (a) and (b) were also evaluated for both sign correction methods separately. Metric (c) was only applied on the complete pipeline.

Conservatively, a scan was evaluated as failure when in one slice the respiratory signal was wrongly estimated.

3. Results

3.1. Performance of the final algorithm

The proposed algorithm was validated in 50 cases from the 5 subjects considered for this study. Fig. 5 shows examples of the estimated respiratory signal derived from the imaging data, for (a) the resting condition and (b) the condition of 50% of maximal exercise intensity, both of the same subject. In both cases, the estimated respiratory signal corresponds well to the ground truth plethysmograph signal.

In the majority of scans high correlation (*metric a*) was found between the estimated and the plethysmograph signals. Fig. 6 shows the correlation coefficients obtained between the plethysmograph signal and the estimated respiratory signal after sign correction (orange squares). In 38 scans (76%) a high correlation was obtained of greater or equal to .7. In 9 scans (18%) a correlation with the plethysmograph signal lower than .5 was obtained.

The results for *metric b*, i.e. success of the sign correction method are shown in Table 1 (column "Combined") and is high and acceptable for all exercise levels.

The results for *metric c* are summerized in Table 2, which specifies the median mean and standard deviation of the differences between peak inspiration and expiration frames from the estimated respiratory signal and the plethysmograph. Overall, the mean error is in the range of 5 to 10 frames with a standard deviation between 5 and 16. The low mean error corresponds to the high correlation between the estimated and the plethysmograph system in 80% of the scans. In addition, Fig. 7 shows the distribution of the error at each of the exercise levels. The data are presented per slice and also overall data per respiratory phase. A slight trend can be observed in the slice-wise error distributions in which a higher error is present in the first and last slices. The outliers observed in all error distributions can be attributed to two main sources, i.e. the difference in peak locations due to slices with opposite sign compared to the plethysmograph signal and the occasional absence of principal components which correctly estimated the respiratory motion. Most of the outliers correspond to the latter category.

3.2. Analysis of the PCA and sign correction components separately

To further understand the cause of failure, we made an optimal sign corrected RRC signal, by using the plethysmograph signal to correct the sign. This would be the signal if the sign correction methods would be perfect. Correlation of the optimal sign corrected RCC with the plethysmograph system is shown in Fig. 6 diamond squares. In 40 scans (80%) the final estimated signal attains correlation coefficients (square marker) equal or near to the optimal sign corrected RRC signal (diamonds).

The reasons for failure of the ten remaining scans and the number of affected slices are summarized in Table 3. From the ten remaining cases where low correlation was observed, 6 cases (6, 24, 34, 39, 44 and 46), corresponding to 12% of the data,

Table 2. Summary table for each of the exercise intensities distinctly at inspiration and expiration phases. Values are expressed in number of frames.

	Inspiration			Expiration		
Exercise intensity	Median	Mean	Std.	Median	Mean	Std.
Rest	5	5.80	5.58	6	8.51	10.70
25%	4	9.01	15.7	3	8.26	14.49
50%	3	6.68	9.48	3	6.72	9.78
66%	2	5.22	7.83	2	5.07	7.39

also showed a poor optimal correlation. In these cases the respiratory signal was not optimally estimated by the RRC (2nd PCA component fails to represent respiratory motion). In 4 scans (14, 25, 40 and 49), representing 8% of the data, the ROI for motion tracking was located incorrectly (Table 3). Hence, the displacement and the sum of the black voxels signals failed to capture (a sufficient part of) the diaphragmatic motion. In this case the RRC was correctly defined, however incorrect location of the ROI made the sign correction more prone to errors. As a result, inspiration phases were mistaken for expiration phases (and vice versa) in some slices, where the sign of the waveform was determined incorrectly.

Table 3 also summarizes the number of slices that were wrongly estimated and the cause. In 12 slices the cause could not clearly be attributed to either non optimal PCA or sign correction method (Incorrect ROI). Hence, the incorrect sign determination has no clear cause, although it might be attributed to an irregular respiratory motion.

In addition a trend of increasing failure at higher exercise intensity was observed.

Improvement of using the combined sign correction method as outlined in the methods section over the two methods separately is shown in Table 1.

3.3. Reliability measures

The results of the ROC analyses for the reliability estimates are given in Table 4. The threshold is defined that if the reliability measure for a slice is lower than this threshold the respiratory signal estimated for the slice is labeled as wrong. For measures $\mathcal{R}^6$ and $\mathcal{R}^7$ the maximal AUC was reached for $t_D = .71$ and $t_B = .62$. The overall best reliability measure is $\mathcal{R}^6_{.71}$ and only misses 6 out of 82 wrongly estimated slices.

4. Discussion

In this work we developed and validated a pipeline to derive respiration signals from ungated cine CMR during intense exercise. We built on similar approaches based on PCA [4] [16] and registration [6] [12] [15], that have been successfully applied successfully on images acquired at rest. To the best of our knowledge, data-driven techniques to

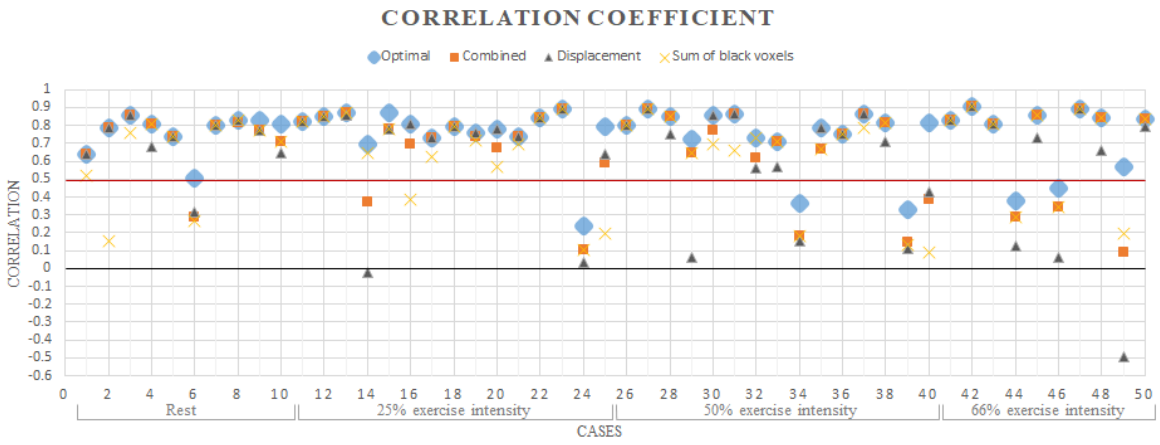

Figure 6. Correlation coefficients between the plethysmograph and the estimated respiratory signals using different sign correction methods. Optimal correlation coefficients below 0.5 were considered as insufficient.

Table 3. Failure corresponding to the cases where non-optimal PCA estimation and incorrect location of the ROI was observed. Failure is expressed by number of slices. The total failure is the number of slices that were incorrectly estimated when the combined sign correction method was applied (Table 1).

Failure	All cause		Non-optimal PCA		Incorrect ROI	
Exercise intensity	Scans	Slices	Scans	Slices	Scans	Slices
Rest	1	8	1	5	-	-
25%	3	22	1	11	2	7
50%	3	29	2	19	1	5
66%	3	23	2	15	1	8
TOTAL	10	82	6	50	4	20
Percentage	20%	9%	12%	61%	8%	24%

extract the respiratory signal have not been applied for different exercise intensities datasets on ungated cine images.

4.1. First principle components

In previous work on PET/CT [16], the respiratory motion was derived form the first principle component. Applying PCA to the ungated cine imaging revealed that the second component was related to respiration. In our application, the first PC forms a signal with a fixed amplitude. This corresponds to the DC component in the frequency domain as is shown in Fig. 2(b). This component is related to the imaging sequence. The difference in signal on the initial frames per slice, where the steady state is not

Table 4. Receiver Operator Characteristics of the reliability measures to estimate erroneous respiratory signal estimation. AUC: Area under the Curve.

measure	threshold	AUC	sensitivity	specificity
$\mathcal{R}^1$	.67	.87	.81	.81
$\mathcal{R}^2$	.68	.90	.88	.87
$\mathcal{R}^3$	.64	.92	.85	.85
$\mathcal{R}^4$	.85	.94	.88	.88
$\mathcal{R}^5$	.52	.87	.79	.80
$\mathcal{R}^6_{.71}$	.77	.96	.92	.92
$\mathcal{R}^7_{.62}$	.79	.94	.88	.88

yet obtained. The spikes shown at the beginning of each slice correspond to the first frames, which are brighter due to the steady state of the acquisition. This is an MRI sequence-related transient, unrelated to any physiological condition.

The second component was determined as the respiration related component.

The third component has some power in the frequency range as well, however to a lesser extent. Hence, it is more complicated to interpret this signal, although it might be attributed to other types of motion (e.g. chest or body motion). It can also be observed that the motion of the heart was not represented by any of the first three PCs (Fig. 2(a)). Moreover, the power spectrum shown in Fig. 2(b) confirms this observation, since it does not show a clear peak within the heart beat frequency range (∼1-2 Hz).

4.2. Data processing

The solution of the problem stated in section 2.4 Eq. (2), depends on the assumptions that can be made about the matrices W and P. Examples are non-negativity (leading to non-negative matrix factorization, NMF), independence (leading to Independent Component Analysis, ICA) and maximal variance and orthogonality (leading to Principal Component Analysis, PCA). Assuming the respiratory motion could be captured in one orthogonal component, we used PCA in our pipeline, since the variation of interest (i.e. respiration) presents a significant portion of the total variance, and is furthermore (approximately orthogonal) to the variation due to the other sources of motion (e.g. heart beating, chest movements).

Using PCA and a sign correction procedure we achieved a good reconstruction of the respiratory signal at rest condition, which was highly correlated with the plethysmograph signal. The results obtained at rest correspond with previous studies [6], where the lowest normalized Root Mean Squared Error between the data-driven signal and the acquired signal was 13.5% for the CT series and 5.9% for the PET series. We obtained a correlation coefficient greater than 0.7 in 84% of the cases. Regarding the sign correction method, at rest we had only 4% of failed slices using the combined

method, whereas in [4] a percentage of failure of 5.3% was observed. Despite the fact that in previous studies the true respiratory motion was acquired with different methods (e.g. optical) and the performance of the algorithms was assessed with a different criteria, the results showed high similarity between the estimated respiratory signal and the acquired respiratory motion signal.

Respiratory signals estimated with our pipeline attained a high correlation with the gold standard plethysmograph signal (Fig. 6) and in most cases the sign of the waveform segments could be correctly determined (Table 1). It has been demonstrated that both the displacement and the sum of the black voxels signals are complementary to determine the correct respiratory motion direction. As expected, combination of both sign correction methods leads to an overall better sign correction than either method individually. However, at rest, 25% and 50% of the maximal exercise intensity the sign correction using the displacement signal performed similar as the combined method. The performance of the algorithm was drastically improved at 66% of the maximal exercise intensity when the combined sign correction criterion was applied. Overall, the sum of the black voxels within the ROI had a higher percentage of failure. Nevertheless few cases showed better correlation with the plethysmograph signal than using the displacement signal as sign correction method, as can be observed in Fig. 6.

High correlation between the displacement signal and the estimated respiratory signal obtained from the PCA algorithm determine in first instance the direction of respiratory motion. However, in some cases minimal or no displacement was observed, especially at the extrema of the stack of slices, in which a much smaller part of the diaphragm is cross-sected. As described in the acquisition protocol (see section 2.3), the first slices correspond to the apex of the heart, whereas the last slices correspond to the base. In these images the diaphragm is less visible and can barely be observed, consequently the sign correction method failed resulting in a higher error. The number of black voxels in an automatically defined ROI was then used to determine the sign of the estimated respiratory signal when the displacement signal delivered low correlation with the estimated signal. For both signals a threshold was defined to determine whether sign correction is required. The thresholds applied in the proposed method correctly determined the sign of the estimated signal in the majority of the cases, however, further analysis would be needed to identify the optimal values which can lead to a reduction of the percentage of failure.

Part of the validation process performed in this work evaluated the correlation between the plethysmograph and the estimated respiratory signals (see Fig. 6). When low correlation is obtained it might be difficult to determine the cause, as it could be due to an imprecise plethysmograph signal or to a non-optimal estimation of the respiratory signal delivered by the PCA algorithm. As the plethysmograph is attached to the body of the subject, it could be sensitive to other types of motion and as result, measure a signal which does not represent the true respiratory motion. During exercise stronger subject motion is expected, and thus the respiratory signal obtained by the plethysmograph is also expected to be imprecise. Therefore, a lack of a gold standard

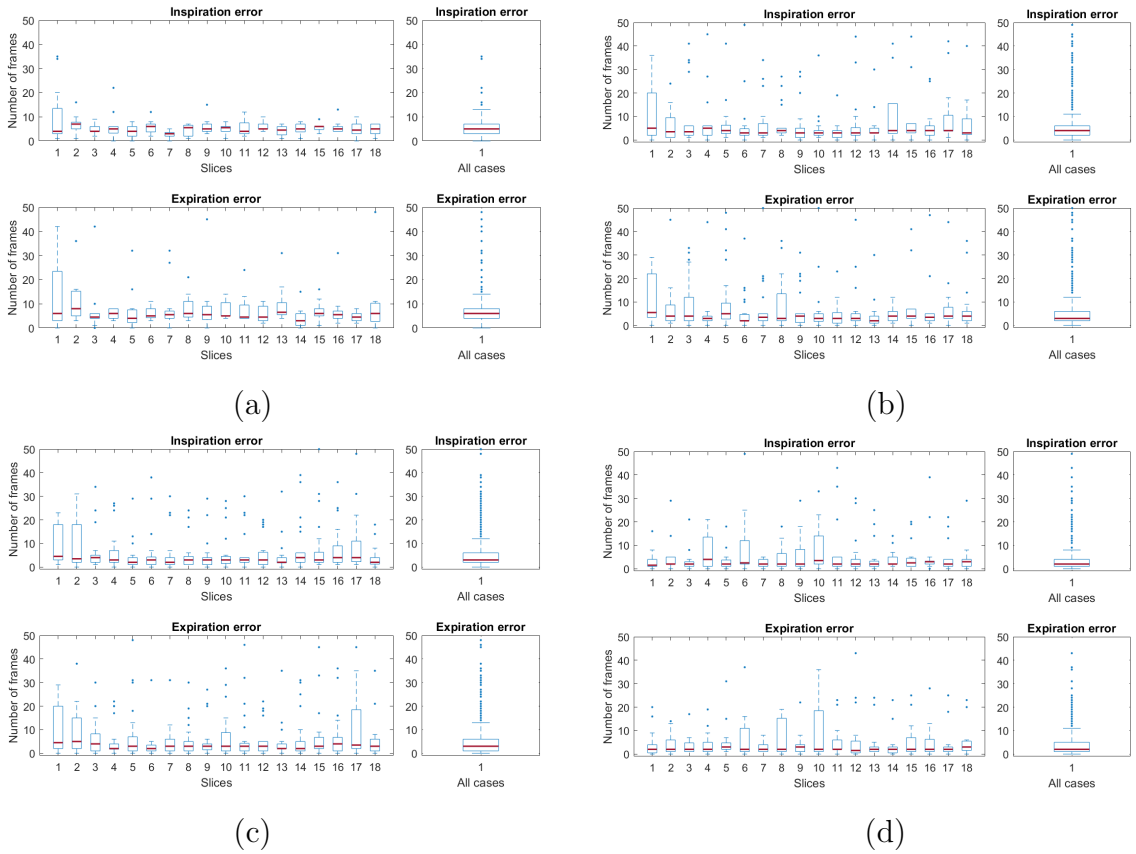

Figure 7. Distribution of error expressed in number of frames at (a) rest, (b) 25%, (c) 50% and (b) 66% of maximal exercise intensity. The range of the Y axis was adjusted to 50 frames for better visualization.

for respiratory motion acquisition could bias the evaluation of the method. However, the plethysmograph signals included in our test set effectively reproduced the respiratory motion in each case, which implies that low correlation between signals corresponded to a non-optimal estimation of the respiratory motion by PCA. Only two plethysmograph signals in the training set showed errors in the measured respiratory motion for certain slices. We acknowledge that spirometry would be a better alternative as gold standard to plethysmography, but it adds additional discomfort to the subject especially during high intensity exercise in the small bore of the magnet.

In our study, the extraction of the respiratory signal at 25%, 50% and 66% of maximal exercise intensity has shown to be feasible. Despite the fact that higher body motion is expected as exercise intensity increases, the algorithm estimated correctly the respiratory motion in the majority of the cases. However, an trend for increase in the percentage of failure as exercise intensity increases was shown in Table 3. This is most likely due to the adverse influence of motion artifacts on PCA estimation. Additionally, it has been observed that respiratory signal estimation is subject dependent, an increase of the body motion of the subject during acquisition leads to an erroneous estimation, hence the percentage of failure is increased.

Only in 6 of the 50 cases the PCA-based pipeline proposed in this work yielded a sub-optimal estimate of the respiratory motion. Failure might be attributed to prominent body movements of the subject during image acquisition. Comparable findings have been described in previous studies [4] [16], where other types of non-respiratory-related motion were considered as a limitation for the respiratory signal extraction.

In addition, an overlapping power spectrum of the first three components was observed for the cases where low optimal correlation was obtained. A possible approach to overcome this problem would be to apply PCA in a more restricted area from each of the images, containing interior organs where motion due to respiration is expected to be more prominent (e.g. diaphragm, heart, liver or stomach). Masking outer regions (e.g. chest), where higher motion is expected during exercise due to subject movements, may improve the performance of the PCA algorithm. An alternative would be to use the same ROI described in section 2.5, and apply PCA using this region throughout each slice.

The performance of the proposed method is drastically improved when PCA delivered a signal which is highly correlated to the plethysmograph signal. Compared to the data shown in Table 1, the percentage of failure at rest was decreased from 4% to 2%, which is comparable with the results obtained in [4], where the failure rates were lower than 3%. In our study, the percentage of failure during exercise is also decreased, at 25% of maximal exercise intensity from 8% to 4%, at 50% from 11% to 4% and at 66% from 13% to 6%. This averages to a failure rate of 4% in total. This demonstrates that the proposed method estimates the correct phase of the respiratory motion with high accuracy when the respiratory signal is correctly estimated by the PCA algorithm.

The percentage of failure shown in Table 3, indicates that 24% of the error is attributed to the wrong location of the ROI. An erroneous location of the boundaries which are expected to be affected by respiratory motion (e.g. between diaphragm and lungs), leads to an incorrect determination of the estimated inspiration and expiration phases. The two reference signals for sign correction within this ROI do not properly correspond to respiratory motion, hence the sign correction method applied to the estimated signal is not adequate. As a result, inspiration phases could be confused for expiration phases, and vice versa.

We suggest that a semi-automatic procedure could increase the performance of the algorithm. A minor interaction of the user placing the region of the interest in the optimal location (e.g. boundary between diaphragm and lungs) could lead to an improvement of the current sign correction method. With this approach, the reference signals for sign correction are expected to correlate well with the respiratory motion and its inspiration and expiration phases. Hence, we can reasonably expect fewer sign correction errors, and, if PCA is only applied on a local patch, a better waveform estimation as well. Another approach could be perform PCA on the separate coil images [18], but needs to be further explored.

Processing time for the proposed algorithm was relatively low, the whole process

for each case takes approximately 19 s on a Core i7, 2.5GHz processor. The algorithm comprises loading the data, data processing, respiratory signal extraction applying PCA algorithm, sign correction procedure and location of inspiration and expiration peaks. Around 40% of the computational time is allocated to median filtering the images, hence the time depends strongly on the applied image preprocessing steps. An optimization of the algorithm could lead to an important reduction of processing time, which could be addressed in future studies. Importantly, the estimation is completely unsupervised, which makes processing time issues less stringent.

Since the aim of the algorithm is to replace the plethysmograph signal, a reliability measure of the estimated respiratory signal to detect errors adds to the robustness of this method. We have analysed the possibility of such a reliability measure based on the correlation coefficients of the RRC and the displacement and lung volume signal. The results are satisfactory in terms of sensitivity and specificity to detect errors. However, a small fraction of errors wold not be detected. However, the resulting signal can always be compared to the diaphragmatic motion on the images. An unreliable plethysmograph signal would in a similar way not be completely detectable without comparison to the images. Further work could improve these reliablity estimates.

4.3. Clinical benefits

The automatic location of end-inspiration and end-expiration phases could represent a valuable tool to clinicians to reduce their workload. At this moment an evaluation through all the frames is needed in order to locate end-inspiration and end-expiration phases. With the proposed method the respiratory phases could be located with high accuracy, hence clinicians could perform the evaluation faster. It is our goal to implement the proposed pipeline in the in-house-developed software (RightVol, KULeuven, Belgium) to evaluate the performance in a clinical environment.

5. Conclusion

In this work a method to extract the respiratory signal from ungated CMR data was proposed and evaluated. PCA and 1D-registration form the basis for the algorithm. An additional signal, the sum of the black voxels within a ROI, which represents changes in lung volume, was also computed for the sign correction procedure. We have shown that our proposed algorithm successfully extracted the respiratory signal during different exercise intensities extending similar approaches applied during rest studies. High correlation between the estimated and the plethysmograph signals was obtained, which infer the potential of our technique to be used in datasets where stronger motion is present.

References

[1] G. Claessen, P. Claus, M. Delcroix, J. Bogaert, A. L. Gerche, and H. Heidbuchel. Interaction between respiration and right versus left ventricular volumes at rest and during exercise: a real-time cardiac magnetic resonance study. *AJP: Heart and Circulatory Physiology*, 306(6):H816–H824, 2014.

[2] Andre La Gerche, Guido Claessen, Alexander Van De Bruaene, Nele Pattyn, Johan Van Cleemput, Marc Gewillig, Jan Bogaert, Steven Dymarkowski, Piet Claus, and Hein Heidbuchel. Cardiac MRI: A new gold standard for ventricular volume quantification during high-intensity exercise. *Circulation: Cardiovascular Imaging*, 6(2):329–338, 2013.

[3] Rongping Zeng, Jeffrey A Fessler, James M. Balter, and Peter A Balter. Iterative sorting for four-dimensional CT images based on internal anatomy motion. *Medical Physics*, 35(3):917–926, mar 2008.

[4] Ottavia Bertolli, Simon Arridge, Scott D. Wollenweber, Charles W. Stearns, Brian F. Hutton, and Kris Thielemans. Sign determination methods for the respiratory signal in data-driven PET gating. *Physics in Medicine and Biology*, 62(8):3204–3220, 2017.

[5] Kate McLeish, Derek L.G. Hill, David Atkinson, Jane M. Blackall, and Reza Razavi. A study of the motion and deformation of the heart due to respiration. *IEEE Transactions on Medical Imaging*, 21(9):1142–1150, 2002.

[6] Paul J. Schleyer, Michael J. O'Doherty, Sally F. Barrington, and Paul K. Marsden. Retrospective data-driven respiratory gating for PET/CT. *Physics in Medicine and Biology*, 54(7):1935–1950, 2009.

[7] Paul J. Schleyer, Michael J. O'Doherty, and Paul K. Marsden. Extension of a data-driven gating technique to 3D, whole body PET studies. *Physics in Medicine and Biology*, 56(13):3953–3965, 2011.

[8] Paul J. Schleyer, Kris Thielemans, and Paul K. Marsden. Extracting a respiratory signal from raw dynamic PET data that contain tracer kinetics. *Physics in Medicine and Biology*, 59(15):4345–4356, aug 2014.

[9] Tinsu Pan, Ting Yim Lee, Eike Rietzel, and George T.Y. Chen. 4D-CT imaging of a volume influenced by respiratory motion on multi-slice CT. *Medical Physics*, 31(2):333–340, jan 2004.

[10] A. P. King, C. Buerger, C. Tsoumpas, P. K. Marsden, and T. Schaeffter. Thoracic respiratory motion estimation from MRI using a statistical model and a 2-D image navigator. *Medical Image Analysis*, 16(1):252–264, jan 2012.

[11] Jinsong Ouyang, Quanzheng Li, and Georges El Fakhri. Magnetic resonance-based motion correction for positron emission tomography imaging. *Seminars in Nuclear Medicine*, 43(1):60–67, jan 2013.

[12] Sergio Uribe, Vivek Muthurangu, Redha Boubertakh, Tobias Schaeffter, Reza Razavi, Derek L.G. Hill, and Michael S. Hansen. Whole-heart cine MRI using real-time respiratory self-gating. *Magnetic Resonance in Medicine*, 57(3):606–613, 2007.

[13] Jan Paul, Evica Divkovic, Stefan Wundrak, Peter Bernhardt, Wolfgang Rottbauer, Heiko Neumann, and Volker Rasche. High-resolution respiratory self-gated golden angle cardiac MRI: Comparison of self-gating Methods in combination with k-T SPARSE SENSE. *Magnetic Resonance in Medicine*, 73(1):292–298, 2015.

[14] Angela O. Leung, Ian Paterson, and Richard B. Thompson. Free-breathing cine MRI. *Magnetic Resonance in Medicine*, 60(3):709–717, 2008.

[15] Christopher W. Roy, Mike Seed, John C. Kingdom, and Christopher K. Macgowan. Motion compensated cine CMR of the fetal heart using radial undersampling and compressed sensing. *Journal of Cardiovascular Magnetic Resonance*, 19(1):1–14, 2017.

[16] Kris Thielemans, Shailendra Rathore, Fredrik Engbrant, and Pasha Razifar. Device-less gating for PET/CT using PCA. In *IEEE Nuclear Science Symposium Conference Record*, pages 3904–3910. IEEE, oct 2011.

[17] Guido Claessen, Andre La Gerche, Thibault Petit, Hilde Gillijns, Jan Bogaert, Mathias Claeys, Steven Dymarkowski, Piet Claus, Marion Delcroix, and Hein Heidbuchel. Right ventricular and pulmonary vascular reserve in asymptomatic BMPR2 mutation carriers. *Journal of Heart and Lung Transplantation*, 36(2):148–156, 2017.

[18] Tao Zhang, Joseph Y. Cheng, Yuxin Chen, Dwight G. Nishimura, John M. Pauly, and Shreyas S. Vasanawala. Robust self-navigated body MRI using dense coil arrays. *Magnetic Resonance in Medicine*, 76(1):197–205, 2016.